Noninterferometric single-shot quantitative phase microscopy

Chao Zuo,[1,2,*] Qian Chen,[1] Weijuan Qu,[3] and Anand Asundi[2]

[1]*Jiangsu Key Laboratory of Spectral Imaging & Intelligence Sense, Nanjing University of Science and Technology, Nanjing, Jiangsu Province 210094, China*

[2]*Centre for Optical and Laser Engineering, School of Mechanical and Aerospace Engineering, Nanyang Technological University, Singapore 639798*

[3]*Centre for Applied Photonics and Laser Technology, Ngee Ann Polytechnic, 535 Clementi Road, Singapore 599489*

**Corresponding author: surpasszuo@163.com*

Received July 15, 2013; revised August 10, 2013; accepted August 10, 2013; posted August 12, 2013 (Doc. ID 193881); published September 5, 2013

We present a noninterferometric single-shot quantitative phase microscopy technique with the use of the transport of intensity equation (TIE). The optical configuration is based on a Michelson-like architecture attached to a nonmodified inverted transmission bright field microscope. Two laterally separated images from different focal planes can be obtained simultaneously by a single camera exposure, enabling the TIE phase recovery to be performed at frame rates that are only camera limited. Precise measurement of a microlens array validates the principle and demonstrates the accuracy of the method. Investigations of chemical-induced apoptosis and the phagocytosis process of macrophages are then presented, suggesting that the method developed can provide promising applications in the dynamic study of cellular processes.

OCIS codes: (180.0180) Microscopy; (110.0180) Microscopy; (100.5070) Phase retrieval; (110.6880) Three-dimensional image acquisition; (100.3010) Image reconstruction techniques.

http://dx.doi.org/10.1364/OL.38.003538

Over the past decade, a great deal of scientific attention has been paid to quantitative phase microscopy, which has emerged as an important tool for phase visualization and structure retrieval of miniature nonabsorbing specimens such as micro-optical elements, unstained cells, and other types of biological and transparent technical samples. Interference techniques, such as digital holography microscopy (DHM), are well established methods for quantitative phase measurement [1], which has been successfully demonstrated in the characterization of microlens arrays [2], investigations of cellular dynamics [3] and drug-induced morphology changes [4]. However, this class of methods typically relies on two-beam interference with a high degree of coherence and, thus, is usually plagued with problems of phase aberration and coherent noise that prevent the accurate phase retrieval and formation of high quality images. Alternatively, the noninterferometric single-beam approaches (specifically, iterative methods [5,6] and transport of intensity equation (TIE) methods [7,8]) use only object field intensities at multiple axially displaced planes without a separate reference beam. In contrast to iterative methods, the TIE is deterministic, requires less intensity measurements, and works well in the case of bright field microscopy with partially coherent sources [8]. Originating from the free-space Helmholtz wave equation, the TIE outlines the relation between object-plane phase and the first derivative of intensity with respect to the optical axis in the near Fresnel region [7],

$$-k\frac{\partial I(\boldsymbol{r})}{\partial z} = \nabla_{\perp}\cdot[I(\boldsymbol{r})\nabla_{\perp}\varphi(\boldsymbol{r})], \tag{1}$$

where k is the wave number, $2\pi/\lambda$, $\boldsymbol{r}$ is the position vector that represents the transverse spatial coordinates (x, y). and $\nabla_{\perp}$ is the gradient operator over $\boldsymbol{r}$. z denotes the optics axis, perpendicular to the x, y plane. Suppose $I(\boldsymbol{r}) > 0$ and, with appropriate boundary conditions, the solution to the TIE is known to exist and be unique [7]. That is, the phase, $\varphi(\boldsymbol{r})$, can be uniquely determined by solving the TIE with determined intensity $I(\boldsymbol{r})$, and longitudinal intensity derivative $\partial I(\boldsymbol{r})/\partial z$. Experimentally, the intensity is easy to obtain. The longitudinal intensity derivative may be estimated by finite differences taken between two close separated images. To acquire the two images with a slight defocus, either the camera or the object has to be manually or mechanically translated, which inevitably slows down the data acquisition speed and thereby limits its applicability to static objects. Techniques based on volume holography [9], chromatic aberrations [10], and flow cytometry [11] have been reported to yield promising TIE phase imaging and eliminate the need for any active elements, manual or mechanical operation, and synchronization of multiple cameras.

In this Letter, we present a novel single-shot quantitative phase microscopy (SQPM) method based on the TIE, with the advantages of instantaneous acquisition, flexibility in defocus distance adjustment, and full compatibility with standard bright field microscopes. Figure 1 shows the experimental configuration wherein a partially coherent white light source with green interference filter (central wavelength $\lambda = 550$ nm) is used for illumination. A commercial inverted bright field microscope (Olympus IX71), which itself is composed of a collector lens, Abbe condenser (0.55 NA) associated with aperture diaphragm, objective, reflective mirror (M_1), and tube lens, produces a magnified image of the specimen at the camera output port (image plane). From the image plane of the microscope, two lenses L_1 and L_2 (focal length $f = f_1 = f_2 = 150$ mm) form a $4f$ system. The image beam is split by a nonpolarizing cube beam splitter (NPBS) into a reflection and a transmission beam. The two beams are then reflected by a spatial light modulator

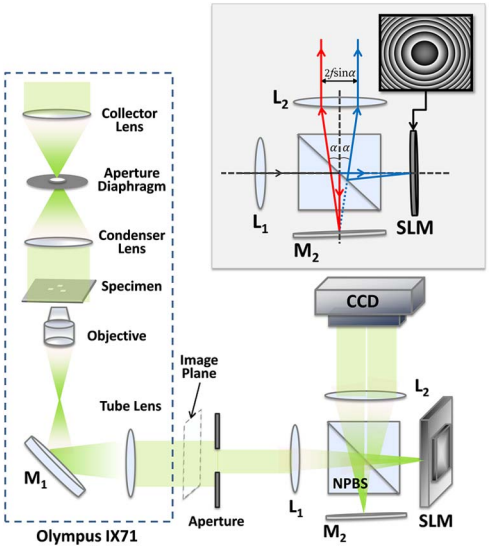

Fig. 1. Experimental setup; NPBS, nonpolarizing beam splitter; M_1, M_2, mirrors; L_1, L_2, lenses; SLM, spatial light modulator. The inset shows one light path along the optical axis with zero local tilt.

(SLM) and a mirror (M_2), respectively, at their Fourier planes. The SLM is a reflective liquid crystal phase-only panel (Holoeye Pluto, 1920 × 1080 pixels with 8 μm pixel size) and was configured to provide full 2π phase modulation with a linear electro-optical characteristic.

To achieve simultaneous capture of two laterally separated images with different defocusing degrees, the normals of mirror M_2 and the SLM both have a small angle, $\alpha \approx 3°$, with respect to the optical axial direction; thus, the two reflected beams are laterally shifted with angular offsets $\pm\alpha$. After passing through the lens L_2, the 2α angular offset is converted to a lateral separation of $2f \sin\alpha$ between the two halves of the images. A rectangular aperture is inserted just behind the image plane of the microscope to ensure the two images are nonoverlapping while maximally filling the camera sensor area. A quadratic phase pattern corresponding to the free space propagation transfer function is displayed on the SLM, further enabling a Δz axially focused shift of the transmission beam. Using a SLM to "digital defocus" the wavefront has been demonstrated on a macroscopic length scale, with applications in smooth wavefront sensing [6,12]. One linear polarizer before the SLM allows high efficiency phase modulation, and a neutral density filter is used to balance the mean intensities reaching the left and right side of the camera (both not shown in Fig. 1). Generally, the optimal propagation or defocus distance for the intensity measurements used in the TIE is object dependent [13,14], related to the maximum physically significant frequency of the specimen as well as the noise level. Without this preknowledge, a searching process is needed to quickly examine the phase resolution and noise profile in order to find the best possible defocus distance for each sample before reconstruction. With our experimental configuration, this can be realized fully automatically by varying the function displayed in the SLM without the need of adjusting the system setup.

The size of the circular condenser aperture diaphragm determines the coherence degree of the Kohler illumination of the SQPM system, which can be represented by the coherent parameter [15,16]—the ratio of the condenser to the objective numerical apertures ($S = \mathrm{NA_{cond}}/\mathrm{NA_{obj}}$). Conventionally, high-resolution optical microscopy depends on the numerical aperture of the condenser being comparable to that of the objective ($S = 0.7 \sim 0.8$). For TIE phase measurements, the results are largely independent of the condenser setting (especially for the low spatial frequency components) [15]. However, in the SQPM, we prefer to narrow down the condenser aperture a bit ($S = 0.3 \sim 0.4$) to ensure a certain level of spatial coherence. This allows a larger depth of field, higher phase contrast on defocus, and, more importantly, a wider linear spatial frequency response range for TIE phase retrieval [15,16].

The numerical processing of the SQPM proceeds as follows. First, accurate registration of the two experimental images is performed. Once the lateral translation between the two halves is obtained, no other calibration procedure is needed for successive measurement unless the setup is changed. Then the intensity derivative is estimated by the finite difference between the two properly registered images. Afterward, the phase map can be calculated by solving the TIE with a fast Fourier transform based Poisson solver. Finally, the background phase, which is measured without the presence of a specimen, is subtracted to get the net phase introduced by the sample only.

To demonstrate the accuracy of the reconstructed phase using the SQPM, we imaged a well-characterized planoconvex microlens array (SUSS MicroOptics, 30 μm pitch) with an Olympus LUCPLFLN 40× 0.6 NA objective. Figure 2(a) shows the raw image of the microlens array obtained in both halves of the camera in a single shot. The left side shows the best focus image, while the right side depicts the defocused one controlled by the SLM. The defocus distance between the two planes was chosen as 8 μm. Figure 2(b) shows the recovered phase by the SQPM. Note that the phase map without 2π discontinuities was directly obtained without phase unwrapping. Figure 2(c) shows the digitally rewrapped phase

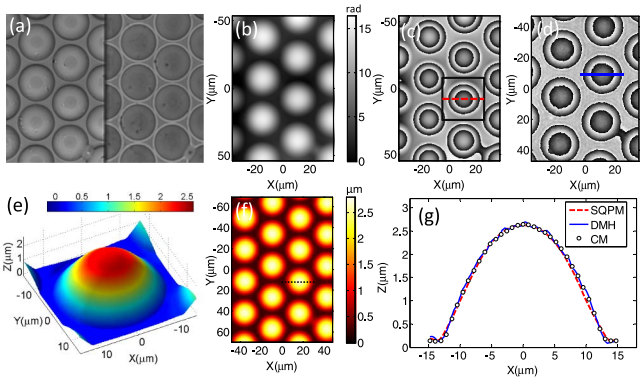

Fig. 2. Experimental results for a microlens array. (a) Raw image obtained in a single-shot; (b) recovered continuous phase by the SQPM; (c) rewrapped phase from (b); (d) wrapped phase map obtained by DHM; (e) 3D profile for one single lens, indicated by the black square in (c); (f) height distribution obtained by confocal microscopy (CM); and (g) lens thickness cross sections corresponding to the line profiles indicated in (c), (d), and (f), respectively.

within the 2π range. The 3D profile of one single lens [indicated by the boxed region in Fig. 2(c)] is shown in Fig. 2(e) by converting the phase to the physical height of the lens. To assess the accuracy of the SQPM phase measurement, the same portion of the specimen was measured using a DHM system [17] (wavelength 650 nm, magnification 43×), and the results were further benchmarked against white-light scanning confocal microscopy (Sensofar PLμ), as shown in Figs. 2(d) and 2(f). Thickness profiles for the same lens from the array taken along the red-dashed line in Fig. 2(c), the blue solid line in Fig. 2(d), and the black-dotted line in Fig. 2(f) are compared quantitatively in Fig. 2(g). The height of the microlens was measured to be 2.46 μm with the SQPM, which is in excellent agreement with the confocal microscopy result of 2.47 μm, demonstrating the quantitative phase retrieval capability of the SQPM. The DHM gave a slightly larger height value (2.54 μm) and the result appears a bit noisy since it suffers from laser speckle noise. In contrast, with the use of partially coherent white light, our approach is completely free of coherent noise. The fitted radius of curvature (ROC) is 407 μm for the SQPM, which slightly overestimated the ROC value compared with the DHM (386 μm), confocal microscopy (389 μm), and the manufacturer specifications (390 μm ± 5%). The small discrepancy can be attributed to the inaccuracies in spatial frequency components for which the finite difference approximation in the TIE does not properly hold, or the imperfection present in the $4f$ imaging system. One should note that, although the continuous phase distribution can be directly recovered with the SQPM even if the phase varies over many multiples of 2π, the TIE is well-posed only if the phase is continuous and single valued. In addition, recovering the phase from its Laplacian inherently assumes that the phase distribution should be a smooth (twice differentiable) function.

An important feature of the SQPM is that the quantitative phase can be recovered with a single image acquisition: thus, it is suitable for studying highly dynamic specimens such as cells. Investigations of live macrophage cells (Raw 264.7) were carried out to demonstrate the potential of the SQPM for the visualization of morphology changes during chemical-induced [poly (diallyldimethylammonium chloride) (PDDA) solution] apoptosis. Adherent macrophages grew overnight at 37°C with 5% CO_2 in the feeding media in a 35 mm × 35 mm dish and then placed in a chamber on the stage of the inverted microscope for time-lapse imaging with an Olympus LUCPLFLN 60× 0.7 NA objective. Unlike before, in this experiment the longitudinal intensity derivative was obtained by the difference between the two images with the same amount but opposite defocus of ±1.5 μm. The central difference could provide a more accurate estimate of the intensity derivative as well as a better tolerance of the spatial incoherence of the illumination [13]. Since live cells approximate pure phase objects, the intensity distribution at the focal plane can be obtained by averaging the two defocused images [15]. Figure 3(a) shows the raw image of a single macrophage cell just before the chemical treatment. The obtained intensity derivative and in focus bright field image are shown in Figs. 3(b) and 3(c), respectively. The intensity derivative demonstrates an isotropic edge enhancement effect, since it is directly related to the Laplacian of the phase, while the in focus bright field image indicates very low contrast, as expected. The recovered phase map is shown in Fig. 3(d), from which we can see that initially the cell was highly ramified with signs of early spreading. Figure 3(e) shows the color-coded 3D rendering of phase maps of the cell undergoing apoptosis at different stages over the whole 2.5 h after the addition of the toxic chemical. The figures below each subimage show corresponding cross sections (labeled by the white dashed line) through the measured phases and optical path length changes. Bear in mind that the constant refractive index ($n_{\text{cell}} = 1.384$, and $n_{\text{medium}} = 1.337$) is

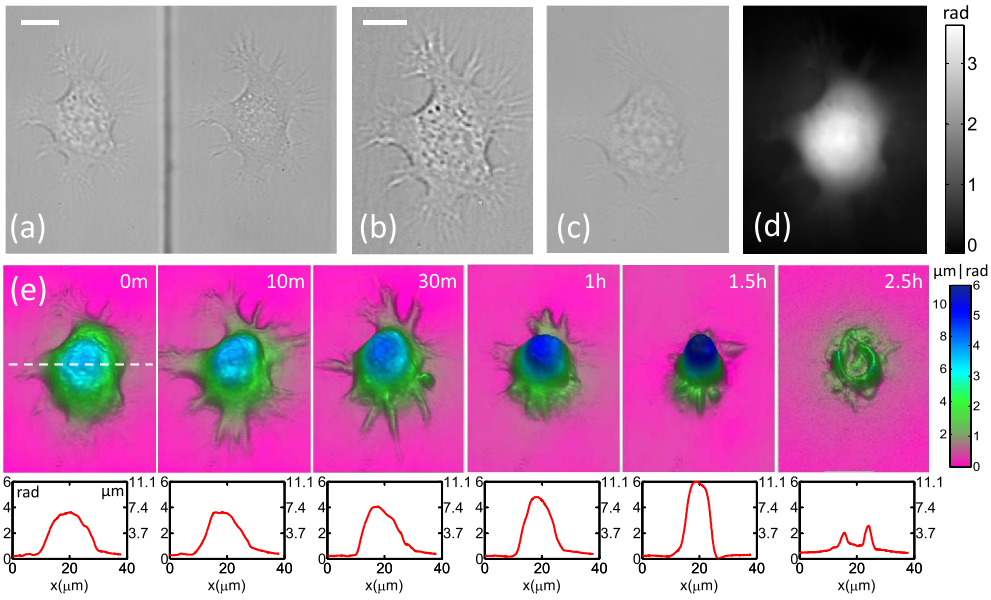

Fig. 3. Morphological changes of a macrophage during chemical-induced apoptosis. (a) Raw image acquired by the SQPM; (b) intensity derivative image; (c) in focus bright field image; (d) retrieved phase map; and (e) color-coded 3D phase distributions (upper row) with phase values and cell thickness cross sections (lower row) in different periods after the addition of PDDA. Scale bar, 10 μm.

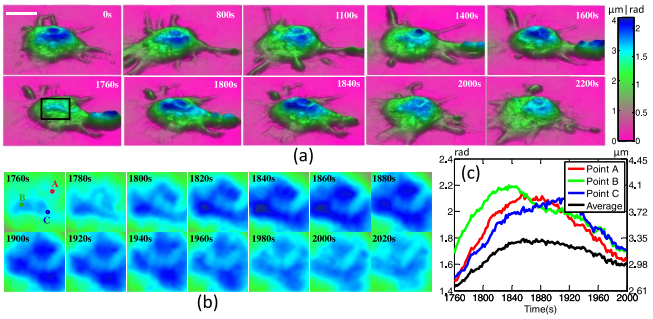

Fig. 4. Study of the macrophage phagocytosis. (a) Color-coded phase profiles at different stages of phagocytosis (Media 1); (b) phase maps of the nuclear region of the macrophage [indicated by the dotted square in (a)] during the internalization stage; (c) phase/thickness variation with time of three points [indicated by the (A) red, (B) green, and (C) blue dots in (b)], and the average of the whole square region (bottom, black curve). Scale bar, 10 μm.

assumed for the entire cell contents, for simplicity, so the thickness profile is directly proportional to the phase profile. From Fig. 3(e) it is obvious that the chemical-induced cell condensation that first started from the nucleus and nuclear membrane, forming an irregular and tightly rolled structure. Afterward, the hallmarks of apoptosis became evident: the cell margin and filopodia progressively shrank, finally contracted into the body, and conglomerated together into a small sphere after 1.5 h, leading to a considerable increase in cell thickness. Finally, the withdrawn cell ruptured and collapsed with a significant decrease of phase delay from 6 rad to less than 2 rad.

As the primary function of macrophage, phagocytosis of foreign bodies found inside the organism is a fascinating and intriguing phenomenon that has attracted remarkable attention. Using the SQPM, the dynamics of the macrophage phagocytosis was investigated. As is shown in Media 1 and Fig. 4(a), we recorded the dynamic process at 0.5 Hz wherein the stages of phagocytosis of the apoptotic cellular debris were distinguishable: recognition and adhesion by actively protruding filopodial, membrane attachment, and, finally, internalization (ingestion and digestion). Figure 4(b) shows the phase distributions of the nuclear region (indicated by the black square in the 1760 s image, 9.3 μm × 9.3 μm) during the internalization stage, which clearly reveals the dynamic changes in cell thickness. The temporal phase changes of three points on the cell, indicated in the first subimage of Fig. 4(b), are further plotted in Fig. 4(c). The black line depicts the average changes within the whole square region. Though the peak positions are different, all curves follow a similar trend: they grow gradually and reach the maximum during the engulfment stage, then progressively decrease during the digestion stage, and finally return to a slightly higher level compared to the beginning. The temporal background phase fluctuation (standard deviation) was measured to be only 0.015 rad, which is negligible compared to the active signals.

In conclusion, we have presented the SQPM, which quantitatively retrieves the phase using an optical setup adaptable to a conventional bright field microscope without any moving parts in a single image acquisition. This offers the possibility of extending the TIE phase imaging to the study of fast moving objects and structural changes in dynamic processes. The investigation of chemical-induced apoptosis and the dynamic phagocytosis process of macrophages demonstrates that the SQPM is a simple, fast, and effective approach for label-free quantitative cell imaging with subcellular resolution. Furthermore, the intrinsic advantages, such as being noninterferometric and unwrapping-free, making it a competitive and powerful alternative to interference techniques for various microscopy applications in micro-optics inspection, life sciences, and biophotonics.

This project was supported by the Research Fund for the Doctoral Program of the Ministry of Education of China (No. 20123219110016), and the Translational R&D and Innovation Fund (TIF) grant of the Singapore Ministry of Education (No. MOE2012-TIF-1-T-003). The authors wish to thank Y. Wang for cell preparation and Prof. A. Kishen from the University of Toronto for clarifications of medical terminology. C. Zuo acknowledges the financial support from the China Scholarship Council (No. 201206840009).

References

1. E. Cuche, P. Marquet, and C. Depeursinge, Appl. Opt. **38**, 6994 (1999).
2. Q. Weijuan, C. O. Choo, Y. Yingjie, and A. Asundi, Appl. Opt. **49**, 6448 (2010).
3. B. Rappaz, P. Marquet, E. Cuche, Y. Emery, C. Depeursinge, and P. Magistretti, Opt. Express **13**, 9361 (2005).
4. B. Kemper and G. von Bally, Appl. Opt. **47**, A52 (2008).
5. G. Pedrini, W. Osten, and Y. Zhang, Opt. Lett. **30**, 833 (2005).
6. C. Falldorf, M. Agour, C. v. Kopylow, and R. B. Bergmann, Appl. Opt. **49**, 1826 (2010).
7. M. Reed Teague, J. Opt. Soc. Am. **73**, 1434 (1983).
8. A. Barty, K. A. Nugent, D. Paganin, and A. Roberts, Opt. Lett. **23**, 817 (1998).
9. L. Waller, Y. Luo, S. Y. Yang, and G. Barbastathis, Opt. Lett. **35**, 2961 (2010).
10. L. Waller, S. S. Kou, C. J. R. Sheppard, and G. Barbastathis, Opt. Express **18**, 22817 (2010).
11. S. S. Gorthi and E. Schonbrun, Opt. Lett. **37**, 707 (2012).
12. P. F. Almoro, L. Waller, M. Agour, C. Falldorf, G. Pedrini, W. Osten, and S. G. Hanson, Opt. Lett. **37**, 2088 (2012).
13. A. V. Martin, F. R. Chen, W. K. Hsieh, J. J. Kai, S. D. Findlay, and L. J. Allen, Ultramicroscopy **106**, 914 (2006).
14. C. Zuo, Q. Chen, Y. Yu, and A. Asundi, Opt. Express **21**, 5346 (2013).
15. E. D. Barone-Nugent, A. Barty, and K. A. Nugent, J. Microsc. **206**, 194 (2002).
16. J. R. Sheppard, J. Opt. Soc. Am. A **21**, 828 (2004).
17. W. Qu, C. O. Choo, V. R. Singh, Y. Yingjie, and A. Asundi, J. Opt. Soc. Am. A **26**, 2005 (2009).